Biochemistry

pubs.acs.org/biochemistry Article

Substrate-Dependent Mobile Loop Conformational Changes in Alkanesulfonate Monooxygenase from Accelerated Molecular Dynamics

Abhishek Thakur, Shruti Somai, Kun Yue, Nicole Ippolito, Dianne Pagan, Jingyuan Xiong, Holly R. Ellis, and Orlando Acevedo*

Cite This: *Biochemistry* 2020, 59, 3582−3593 Read Online

ACCESS | Metrics & More | Article Recommendations | Supporting Information

ABSTRACT: Substrate-induced conformational changes present in alkanesulfonate monooxygenase (SsuD) are crucial to catalysis and lead to distinct interactions between a dynamic loop region and the active site. Accelerated molecular dynamics (aMD) simulations have been carried out to examine this potential correlation by studying wild-type SsuD and variant enzymes bound with different combinations of reduced flavin ($FMNH_2$), C4a-peroxyflavin intermediate ($FMNOO^-$), and octanesulfonate (OCS). Three distinct mobile loop conformations were identified: "open", "closed", and "semiclosed". The substrate-free SsuD system possessed a wide opening capable of providing full access for substrates to enter the active site. Upon binding $FMNH_2$, SsuD adopts a closed conformation that would prevent unproductive oxidation reactions in the absence of OCS. Two salt bridges, Asp111-Arg263 and Glu205-Arg271, were identified as particularly important in maintaining the closed conformation. Experimental substitution of Arg271 to Ala did not alter the catalytic activity, but the variant in the presence of reduced flavin was more susceptible to proteolytic digestion compared to wild-type. With both $FMNH_2$ and OCS bound in SsuD, a second conformation was formed dependent upon a favorable $\pi-\pi$ interaction between His124 and Phe261. Accordingly, there was no observed activity with the F261W SsuD variant in steady-state kinetic assays. This semiclosed conformation may be more appropriate for accepting O_2 into the binding pocket and/or may properly orient the active site for the ensuing oxygenolytic cleavage. Finally, simulations of SsuD simultaneously bound with $FMNOO^-$ and OCS found an open mobile loop region that suggests alternative flavin intermediates may participate in the reaction mechanism.

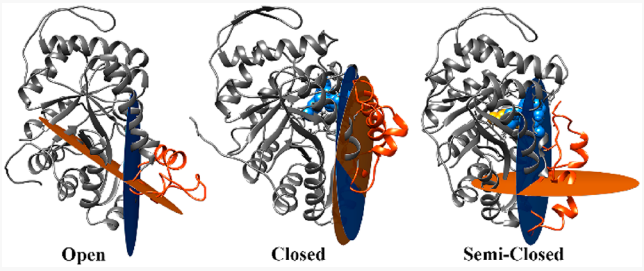

Under limiting sulfur conditions, bacterial organisms express sulfonate-sulfur-utilization (ssu) proteins that allow them to assimilate alternative organic sulfonates and sulfate esters.[1,2] Of specific interest here is alkanesulfonate monooxygenase (SsuD), a flavin-dependent enzyme that performs oxygenolytic cleavage of 1-alkanesulfonates ranging in length from one to ten carbons to yield a sulfite product and corresponding aldehyde (Figure 1).[3,4] The catalytic mechanism involves a reduced flavin ($FMNH_2$) and the activation of dioxygen to form a C4a-(hydro)peroxyflavin intermediate ($FMNOO^-$) that is responsible for breaking the carbon−sulfur bond.[5−8] Composed of a two-component system, FMN-dependent reductase (SsuE) provides $FMNH_2$ to SsuD through a reduction of FMN involving NAD(P)H (Figure 1).[9−11] The large contrast between the binding of $FMNH_2$ to SsuE and SsuD with reported dissociation constants (K_d) of 15.5 ± 1.3 μm and 0.32 ± 0.15 μm, respectively, suggests an immediate release and transfer of the reduced flavin upon formation.[7] Subtle protein−protein interactions between the reductase and oxygenase components promote the direct transfer of $FMNH_2$ from SsuE to SsuD.[12−14]

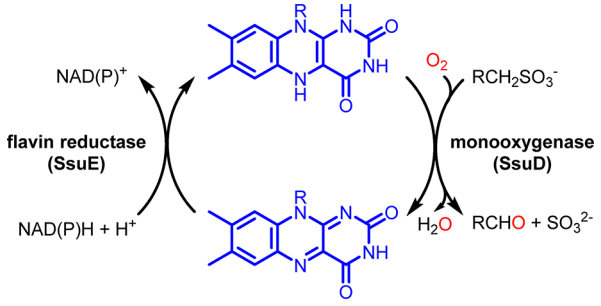

Figure 1. General mechanism for a two-component FMN-dependent monooxygenase system.

Received: July 31, 2020
Revised: September 2, 2020
Published: September 3, 2020

https://dx.doi.org/10.1021/acs.biochem.0c00633
Biochemistry 2020, 59, 3582−3593

The SsuD enzyme is structurally similar to the bacterial luciferase family despite a relatively low amino acid sequence identity; all family members form a triosephosphate isomerase (TIM)-barrel fold with the active site located at the C-terminal end of the β-barrel.[15−18] An insertion sequence has been identified in SsuD (Glu233−Asp307) that contains a dynamic loop near the putative active site.[15] In other TIM-barrel proteins, these mobile loops protect reactive intermediates from the bulk solvent and prevent the release of catalytic intermediates.[19−22] The SsuD dynamic loop region is highly conserved based on sequence alignments of different homologues, and its partial deletion yielded catalytically inactive enzymes despite no overall gross changes in secondary structure and the continued ability to bind reduced flavin.[23] Similar to the bacterial luciferase family, the SsuD loop has been proposed to undergo a lid-gating conformational change following the binding of substrates. For example, an $FMNH_2$-induced conformational change was found to be essential for the subsequent binding of octanesulfonate in SsuD.[6,7,24,25] Rapid kinetic analyses of the reductive and oxidative half-reactions indicated that the SsuD mobile loop deletion variants failed to shield reduced flavin from unproductive oxidation, highlighting the importance of the dynamic loop region for the protection and stabilization of $FMNH_2$.[23]

A conserved arginine residue (Arg297) located in the mobile loop insertion sequence significantly contributes to catalysis as well, as the R297C and R297A SsuD variants had no observable activity and the R297K variant substantially lowered the k_{cat}/K_m value relative to wild-type.[6,15] Interestingly, Arg297 is positioned away from the active site in the reported crystal structure, requiring a conformational change in order to be catalytically relevant.[15] Computational studies have proposed that active site accessibility may be driven by salt bridge formation involving Arg297 and Glu20 or Asp111.[26] However, similar k_{cat}/K_m values as wild-type were reported for the E20A and D111A SsuD variants bringing into question the exact role of the salt bridges during the desulfonation mechanism.[5] Alternatively, molecular dynamics (MD) simulations found that Arg297 may interact with the PO_4^{2-} group of the reduced flavin in a similar fashion to long-chain alkane monooxygenase (LadA), where the loop region was shown to coordinate to the phosphate group of FMN.[5,18]

It is clear that substrate-induced conformational changes present in SsuD are crucial to catalysis, but given the uncertainly of the exact role of the dynamic loop region and the difficulty in crystallizing the insertion region, atomistic-based simulations may be essential for providing further insight. Our previous computational studies found a highly active and flexible mobile loop region, but no evidence of a lid-gating conformational change, possibly a consequence of a short simulation, i.e., 300 ns of unbiased MD.[5] Advanced sampling methods are generally required to find such large structural changes during simulations.[27,28] Hence, accelerated molecular dynamics (aMD)[29] simulations of 1000 ns, which is approximately equal to 2 ms of unbiased brute force MD,[30] were performed here at atomic resolution for each of the following wild-type SsuD systems: (1) substrate-free, (2) with $FMNH_2$, (3) with $FMNH_2$ and octanesulfonate (OCS), and (4) with the C4a-peroxyflavin intermediate ($FMNOO^-$) and OCS. Extensive analysis has been carried out to evaluate the role of amino acid residues located within the mobile loop region that were found to be important to catalysis. Additional simulations featuring single and double residue substitutions located in the active site and on the mobile loop were performed to further clarify the role of key amino acids. These simulations validated with experimental findings provide a clearer understanding of how different combinations of substrates bound in the active site induce multiple conformations of the mobile loop important for catalysis.

MATERIALS AND METHODS

Computational Methods. *Enzyme Preparation.* Starting Cartesian coordinates for the SsuD structures were constructed using a crystal structure possessing a 2.3 Å resolution (PDB ID: 1M41).[15] The reported structure was lacking internal residues 250−282 and C-terminal residues 362−380 and, as such, residues 250−282 were inserted using a comparative modeling program MODELLER 9.10.[31] The program generated a refined 3D model of the given protein sequence (target) based primarily on its alignment to one or more proteins of known structure (templates). The templates used were the SsuD structure (PDB ID: 1NQK) and the structure of the luciferase-like monooxygenase from *Bacillus cereus* (PDB ID: 3RAO). The $FMNH_2$ ligand was inserted into the active site region of SsuD based on a superposition with coordinates from a LadA enzyme with a bound FMN (PDB ID: 3B9O).[18]

Autodock Vina. Inserting octanesulfonate into SsuD was performed using AutoDock Vina.[32] A grid box was fit to encompass the proposed active site, where between 10 and 20 binding modes were analyzed to determine the most probable structure based on previously proposed catalytic sites.[6,15,25] Standard flexible protocols of AutoDock Vina using the Iterated Local Search global optimizer algorithm were employed to evaluate the binding affinities of the substrates within SsuD. All active site residues, as defined by the box size used for the receptors, were set to be rotatable. Calculations were performed using the exhaustiveness of the global search set to 100, a number of generated binding modes set to 20, and a maximum energy difference between the best and the worst binding modes set to 5.

aMD Protocol. Accelerated molecular dynamics (aMD) simulations were performed on the wild-type SsuD monomer with four different combinations of bound substrates. The aMD technique adds a bias potential that surmounts high energy barriers and only requires the evolution of a single copy of the system, i.e., does not require advanced information on the location for either the potential energy wells or saddle points. The bias boost potential function $\Delta V(\mathbf{r})$, which is a continuous positive value, is introduced whenever the true potential value $V(\mathbf{r})$ gets below a certain chosen energy value (E), and the simulation is performed using the modified potential $V^*(\mathbf{r}) = V(\mathbf{r}) + \Delta V(\mathbf{r})$.[29,33,34] When the true potential function $V(\mathbf{r})$ is greater than E, the simulation is performed on the true potential, $V^*(\mathbf{r}) = V(\mathbf{r})$. The minima and the barriers are still maintained, thereby conserving the shape of the real potential, which is recovered by a reweighting procedure.[35] Boost parameters E and α for dihedral boost were derived from a 10 ns trajectory of an unbiased MD simulation following a recommended best-practices procedure.[36]

The SsuD systems were fed into the leap module of the Amber package,[37] where the appropriate hydrogen atoms were added. The enzyme was solvated in a box of explicit TIP3P water molecules[38] extending at least 10 Å beyond the enzyme, and sodium ions were added to maintain charge neutrality. The Amber force field[39,40] was used to construct the topology files for the protein, while the parameters for the ligands were

https://dx.doi.org/10.1021/acs.biochem.0c00633
Biochemistry 2020, 59, 3582−3593

obtained from the generalized amber force field (GAFF).[41] Each ligand was optimized by carrying out a Monte Carlo conformational search using the BOSS program[42] and the OPLS force field.[43] The lowest energy structures were reoptimized at the MP2/6-31G(d) theory level using Gaussian 09 software[44] and the lowest energy MP2 structure was used to determine the restrained electrostatic potential (RESP) partial atomic charges using HF/6-31G(d) and the AmberTools antechamber module.[37]

For each system, the initial structure was conjugate gradient (CG) minimized for 200 steps for the water molecules, followed by 10000 steps of CG optimization of the entire system to remove poor contacts. After minimization, the full system was gradually heated from 0 to 300 K using a constant NVT ensemble for 50 ps of MD using the weak-coupling algorithm with a temperature coupling value of 2.8 ps. The system was then switched to a constant NPT ensemble at 300 K and 1 atm using a coupling value of 2.0 ps for both temperature and pressure and ran for 500 ps. Finally, the system was returned to NVT and equilibrated for an additional 500 ps. Following equilibration, 10 ns of production data was collected at constant NVT for each protein complex. Accelerated molecular dynamics was then performed for 1000 ns on each SsuD complex using the GPU-accelerated version of AMBER 16.[45,46] Two additional production runs of 300 ns were performed on each SsuD complex featuring unique trajectories that began from starting structures derived from clustering analysis of the original 1000 ns runs. Standard deviations were computed using the three production runs. All MD simulations utilized the particle mesh Ewald method to compute the long-range Coulomb force, periodic boundary conditions with a nonbonded cutoff distance of 12 Å, and a time step of 1.0 fs.

Computational Analysis. Conformational changes in the SsuD enzyme were analyzed using root-mean-square fluctuation (RMSF), which calculates the positional deviations over time relative to a reference structure. Root-mean-square deviation (RMSD) calculations were carried out by (1) comparing backbone protein atoms (N, C_α, and C) distance deviations relative to the first frame over time and (2) by comparing each snapshot in the trajectory with respect to all others using the MDAnalysis program.[47] Clustering, hydrogen bond analysis, and distance calculations were carried out using the ptraj and cpptraj programs.[48] For the clustering calculations, the average-linkage algorithm was utilized.[49]

EXPERIMENTAL METHODS

Materials. All chemicals for purification and protein assays were purchased from Sigma-Aldrich, Fischer, Bio-Rad, or Fluka. *Escherichia coli* strains (XL-1 and BL21(DE3)) were purchased from Stratagene (La Jolla, CA). Plasmid vectors and pET21a were obtained from Novagen (Madison, WI). DNA primers were synthesized by Invitrogen (Carlsbad, CA). All UV−vis absorbance spectra were recorded using an Agilent Technologies diode array spectrophotometer (model HP 8453).

Construction, Expression, and Purification of Recombinant Proteins. A recombinant pET21a plasmid containing the *ssuD* gene was used to construct variants of the SsuD enzyme. Primers for each variant were designed as 33 base oligonucleotides containing the desired substitution. The CGG codon and the CGA codon for R263 and R271, respectively, were replaced by GCG (R263A) and GCA (R271A). The TTC codon for F261 was replaced with TGG (F261W). The Qiagen kit plasmid purification protocol was utilized to prepare the SsuD plasmid for site-directed mutagenesis. The constructed variants were confirmed through DNA sequencing analysis by Eurofins Genomics (Louisville, KY). Each plasmid containing the substituted *ssuD* gene was transformed into *E. coli* BL21(DE3) supercompetent cells (Invitrogen, CA) for protein expression. The expression and purification of the variants and wild-type SsuD proteins were performed as previously described.[8] Following purification, stocks of the variants and wild-type SsuD enzymes were stored in 25 mM potassium phosphate (pH 7.5), 100 mM NaCl, and 10% glycerol at −80 °C. The SsuD concentration was determined spectrophotometrically using a molar absorption coefficient of 47900 M^{-1} cm^{-1} at 280 nm. Wild-type SsuE was also expressed as previously described, and the concentration was spectrophotometrically determined using a molar absorption coefficient of 20340 M^{-1} cm^{-1} at 280 nm.[8]

Steady-State Kinetic Analysis. A coupled assay monitoring the sulfite production was used to determine steady-state kinetic parameters of the variants and wild-type SsuD as described previously.[2] The reactions were initiated with the addition of NADPH (500 μM) into a reaction mixture containing SsuD or the variants (0.2 μM), SsuE (0.6 μM), FMN (2 μM), and varying concentrations of octanesulfonate (0−1000 μM) in 25 mM Tris-HCl (pH 7.5) and 0.1 M NaCl at 25 °C. The reaction was quenched after 3 min with 8 M urea followed by the addition of DTNB (1 mM). After the addition of DTNB, the reaction was allowed to develop at room temperature for 2 min, and the absorbance was measured at 412 nm using a molar extinction coefficient for the TNB anion of 14100 M^{-1} cm^{-1}. All assays were performed in triplicate, and steady-state kinetic parameters were determined by fitting the data to the Michaelis−Menten equation.

Limited Proteolytic Analysis. The susceptibility of the variants and wild-type SsuD to proteolysis was investigated at room temperature in the presence of FMN and $FMNH_2$. Individual samples of R263A, R271A, R263A/R271A, and wild-type SsuD (15 μM) were prepared in 200 mM ammonium bicarbonate/1 mM $CaCl_2$ (pH 8.4) and treated with TLCK-treated chymotrypsin (10 μg/mL). The concentration of FMN in each reaction mixture was 20 μM. Chymotrypsin stock solution (1 mg/mL) was prepared in 1 mM HCl/1 mM $CaCl_2$ (pH 8.4). After the addition of chymotrypsin, samples (10 μL) were taken at various times (0 s, 1 min, 5 min, 7 and 10 min) and added to 2 μL PMSF (6 mg/mL) in 100% isopropanol to quench the reaction. The degree of proteolysis of each sample was analyzed by SDS-PAGE.

To measure the degree of proteolysis in the presence of $FMNH_2$, an anaerobic solution of FMN (200 μM) was made in 25 mM potassium phosphate (pH 8.0), 20 mM EDTA, and 10% glycerol. The FMN solution was bubbled with argon gas for 30 min before being transferred to an anaerobic chamber. After the addition of glucose (10 mM) and glucose oxidase (0.1 μM), both protein and FMN solution were incubated in an anaerobic glovebox to remove trace amounts of dioxygen. The anaerobic FMN solution was photoreduced inside a gastight Hamilton syringe with a long-wavelength UV lamp. The concentration of $FMNH_2$ in each reaction mixture was 20 μM, and the concentration of protein was 15 μM when included in the reaction. With both $FMNH_2$ and octanesulfonate included in the reaction, the octanesulfonate concen-

https://dx.doi.org/10.1021/acs.biochem.0c00633
Biochemistry 2020, 59, 3582−3593

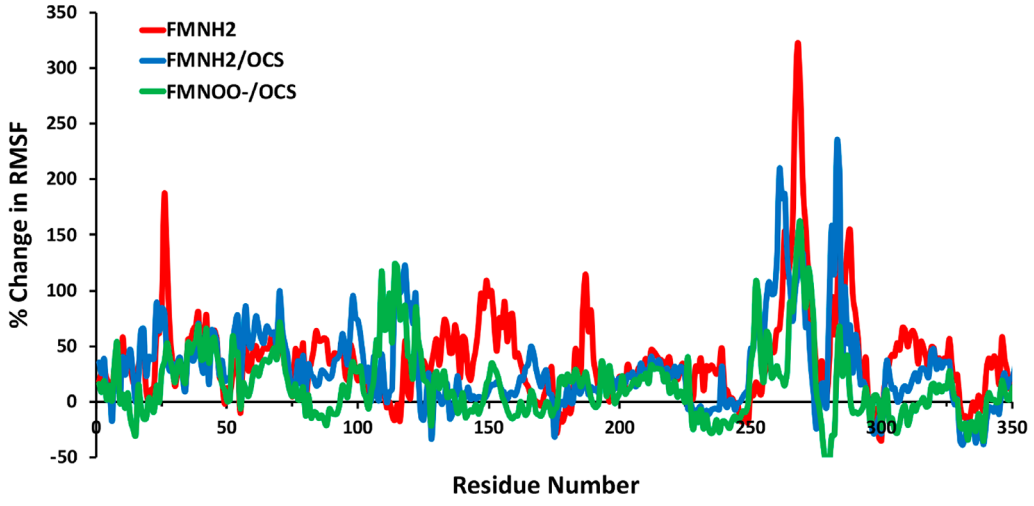

Figure 2. Average percent change in root-mean-square fluctuations (RMSF) of the SsuD C_α backbone atoms upon binding substrates relative to substrate-free SsuD. A positive change in RMSF signifies that residues have become more localized upon substrate binding, and a negative change is indicative of enhanced fluctuations.

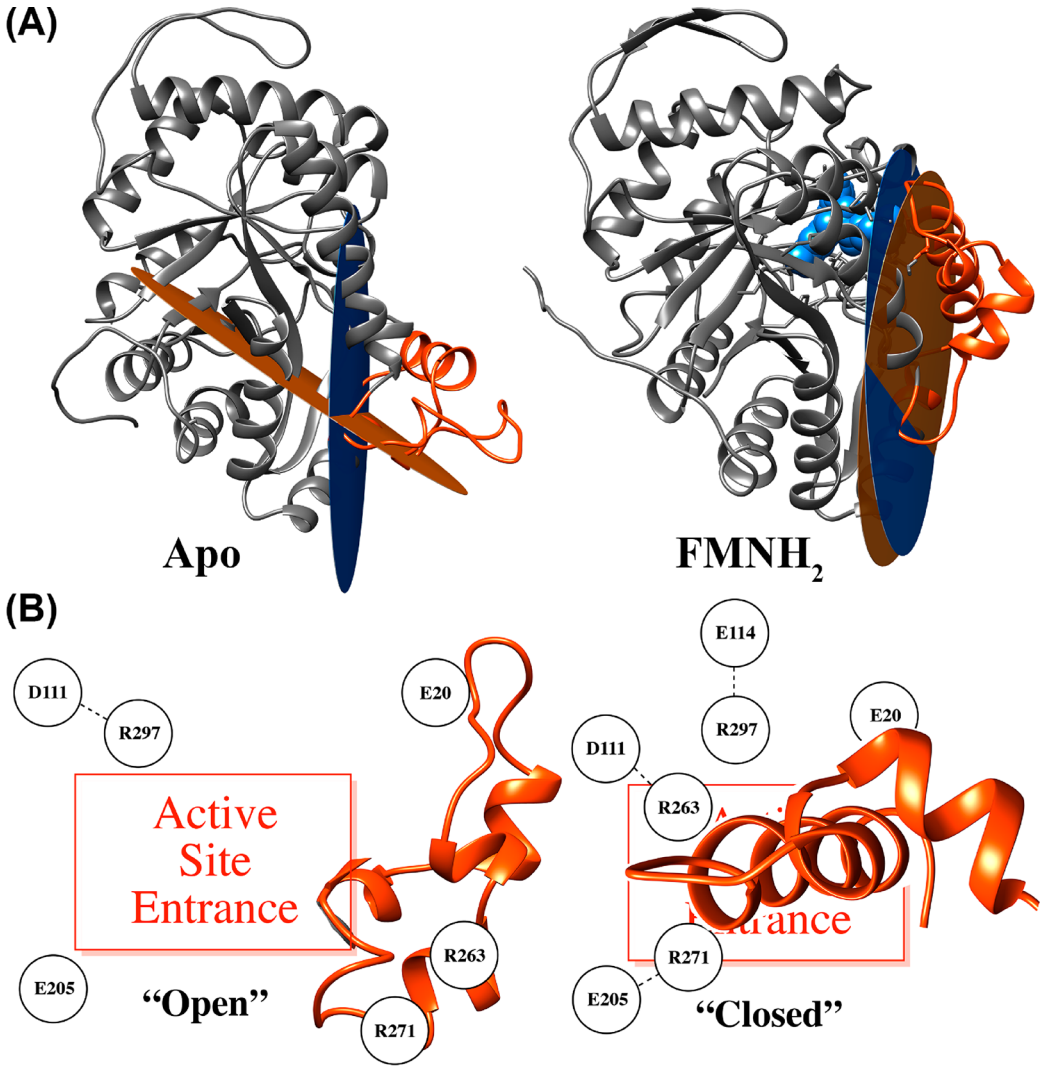

Figure 3. (A) Top cluster structures for the substrate-free and $FMNH_2$-bound SsuD complexes from the 1000 ns aMD simulations. The mobile loop plane (D111-K204-L289) was colored in orange and the active site entrance plane (I246-Q269-L289) in blue. (B) Cartoon representation of key active site and mobile loop residue interactions in the open and closed SsuD conformations.

https://dx.doi.org/10.1021/acs.biochem.0c00633
Biochemistry 2020, 59, 3582−3593

tration was 150 μM. After the addition of chymotrypsin, samples (10 μL) were taken at various times (0 s, 1, 5, 7, and 10 min) and added to 2 μL of PMSF (6 mg/mL) in 100% isopropanol to quench the reaction. The degree of proteolysis of each sample was analyzed by SDS-PAGE.

RESULTS AND DISCUSSION

SsuD Structure Analysis. Root-mean-square deviations (RMSD) were computed for the aMD simulations of each SsuD system bound with (1) substrate-free, (2) $FMNH_2$, (3) $FMNH_2$ and OCS, and (4) $FMNOO^-$ and OCS. The structural stability of each simulation was monitored using two different RMSD analysis techniques: (i) comparing protein backbone atoms distance deviations relative to the first frame over time and (ii) taking the RMSD between all pairs of frames (Figure S1).[50] It was found that the RMSD values of the backbone protein atoms yielded a steady average value for all complexes, particularly after approximately 300 ns of the 1000 ns production run (Figure S1). This suggests that any major substrate-induced conformational changes within the enzyme[24] may have been completed by 300 ns. The effects of substrate binding upon enzyme dynamics were further investigated using a root-mean-square fluctuation (RMSF) analysis on the SsuD backbone atoms. The average percent change in the RMSF between different combinations of substrates bound to SsuD relative to substrate-free is given in Figure 2. Upon binding the substrates, any residues that become more localized will have a positive change in RMSF, whereas residues that have become more flexible will exhibit a negative change. A review of the RMSF percent change indicates the region most affected by substrate binding encompassed residues 250−300, which is to be expected given that residues 250−282 make up the highly active and flexible mobile loop. In addition, two other enzyme regions, residues 10−30 and 100−200, possessed significant positive peaks. These regions within SsuD contain amino acids that have been suggested to drive conformational changes via salt bridge formations, i.e., Arg297, Glu20, and Asp111,[26] and contain residues that interact directly with the bound FMN and octanesulfonate.

Clustering analysis was performed on the aMD trajectories in order to identify the most dominant structures for each SsuD system. The top cluster for the substrate-free SsuD simulation is characterized by a fully "open" conformation with regards to the mobile loop region for 64% of the simulation. Interestingly, when SsuD is bound solely with $FMNH_2$, the most dominant cluster was found to be a "closed" conformation where the mobile loop spontaneously covered the binding pocket entrance for 75% of the 1000 ns trajectory. This is similar to reported replica exchange simulations of bacterial luciferase, where closed mobile loop conformations were only visited when bound with $FMNH_2$.[28] The addition of OCS to the SsuD binding pocket cobound with $FMNH_2$ gave a preference for a "semiclosed" conformation with the most dominant cluster encompassing 61% of the trajectory. Intriguingly, the combination of $FMNOO^-$ and OCS gave a conformation for 70% of the simulation time that appeared to be partially open, and the C4a-peroxyflavin intermediate exited the active site after ∼900 ns. The definition of open, closed, and semiclosed conformations for SsuD will be discussed in greater detail further below.

Two additional 300 ns trajectories (runs 2 and 3) were computed for each SsuD system using starting coordinates derived from the most dominant cluster in each of the previous 1000 ns aMD simulations (run 1). For example, the SsuD system bound to $FMNH_2$ used the closed conformation (see Figure 3) as the initial Cartesian coordinates for simulations in runs 2 and 3. However, each additional run was not a continuation of the original 1000 ns run, but instead featured an independent minimization, equilibration, and production run as described in the methods section. Unsurprisingly, the most dominant cluster identified during runs 2 and 3 matched the conformation of run 1 for all SsuD systems, i.e., apo, $FMNH_2$, $FMNH_2$/OCS, and $FMNOO^-$/OCS. Figures and PDB structures for all the SsuD systems are available in the Supporting Information.

Open vs Closed Conformation. With regard to mobile loop conformations, the role of Arg297 is noteworthy. This conserved residue is located in the mobile loop insertion sequence and directly facilitates the catalytic activity of SsuD as its substitution to a lysine or alanine leads to deterioration of observed activity.[6] Arg297 is believed to stabilize the flavin and/or favorably interact with protein residues responsible for the loop-closure movement.[5] Notably, earlier computational studies by Ferrario et al. performing 20 ns of unbiased MD on SsuD have shown that the formation of a salt bridge between Arg297 and Asp111 or Glu20 may help determine the closed or open state of the mobile loop.[26] Their simulations on the substrate-free (or apo) SsuD system found the enzyme would frequently switch between the Arg297-Asp111 and Arg297-Glu20 salt bridges, with no clear preference. However, that study lacked the mobile loop residues 250−282, which have been modeled into the simulated SsuD complexes in this work.

To formalize the definition of an open and closed mobile loop conformation, a dihedral angle was calculated by choosing five points near the active site entrance and on the mobile loop of the SsuD system. Specifically, the mobile loop plane was defined by the C_α atoms of Ile246, Gln269, and Leu289 (colored in orange), and the second plane that defined the entrance of the active site was created by selecting the C_α atoms of Asp111, Lys204, and Leu289 (colored in blue). The common point between the two planes was Leu289. A computed obtuse angle of 122.8° between the two planes of the most dominant cluster (Table 1) for the substrate-free SsuD enzyme implies a wide opening capable of providing full access for substrates to enter the active site. The second and third most dominant clusters for the substrate-free SsuD enzyme gave dihedral angles of 128.9° and 140.4°, respectively. The top 3 clusters encompassed 92% of the entire simulation. Upon binding $FMNH_2$ in SsuD, a substantial overlap between the planes was found with an acute angle of 7.8° calculated. A simple visual check of the apo and reduced flavin-bound 1000 ns aMD cluster structures clearly show an open and closed active site, respectively (Figure 3A).

Table 1. Computed Dihedral Angle (in Degrees) between the Active Site Plane (D111-K204-L289) and the Mobile Loop Plane (I246-Q269-L289) for the Wild-Type SsuD Systems

bound in SsuD	angle	conformation
substrate-free	122.8	open
$FMNH_2$	7.3	closed
$FMNH_2$/OCS	89.5	semiclosed
$FMNOO^-$/OCS	66.8	

https://dx.doi.org/10.1021/acs.biochem.0c00633
Biochemistry 2020, 59, 3582−3593

The most dominant cluster structures from the triplicate aMD runs (Figures S2−S4) were utilized to compute average distances between active site and mobile loop residues in the open apo and closed $FMNH_2$-bound SsuD systems. Multiple residues that include Arg297, Asp111, Arg271, Arg263, Glu205, and Glu114, were identified by the simulations to play a significant role in determining the SsuD mobile loop conformations. Table 2 provides the lengths between the side-chain carbonyl carbon atom on Glu/Asp and the side-chain carbon atom centered in the guanidino group of Arg. The open apo system had a salt bridge interaction between Asp111 and Arg297 with an average length of 6 ± 3 Å. Accordingly, a hydrogen bond population analysis over the entire 1000 ns apo SsuD trajectory found that Arg297 and Asp111 maintained an 81% hydrogen bond percent occupancy with an average H-bond distance of 2.8 Å (Figure 4 and Table S1). Arg297 also formed an additional ionic interaction with the nearby Glu198 residue for 42−44% of the substrate-free SsuD trajectory with an average distance of 2.8 Å. Interestingly, a very large distance of 23 ± 2 Å between Arg297 and Glu20 was computed, which refutes prior suggestions that this salt bridge is important for maintaining an open conformation.[26]

Table 2. Average Distances (in Å) between Residues for the Most Dominant Substrate-Free and Bound Wild-Type SsuD Cluster Structures

	Apo	$FMNH_2$	$FMNH_2$/OCS	$FMNOO^-$/OCS
Asp111-Arg297	6 ± 3	9 ± 1	3.9 ± 0.2	11.8 ± 0.5
Glu20-Arg297	23 ± 2	8 ± 2	18 ± 2	6 ± 3
Glu114-Arg297	13 ± 1	6 ± 2	6 ± 1	12 ± 2
Asp111-Arg263	29.0 ± 0.5	4.0 ± 0.2	17.4 ± 0.2	28 ± 5
Glu205-Arg271	19 ± 2	4.0 ± 0.2	14 ± 2	15 ± 2
His124-Phe261	28 ± 1	21 ± 5	5 ± 1	18 ± 6

As the mobile loop closed over the active site region in the $FMNH_2$-bound system, the Arg297 residue moved to interact with the Glu114 residue at a distance of 6 ± 2 Å (compared to 13 ± 1 Å for substrate-free) and was located roughly in between the Asp111 and Glu20 residues with interacting distances of 9 ± 1 and 8 ± 2 Å, respectively (Table 2). A hydrogen bond occupancy analysis found a H-bond interaction between Glu114 and Arg297 for 41% of the 1000 ns $FMNH_2$-bound SsuD trajectory with an average distance of 2.8 Å (Figure 4 and Table S1). In addition, Glu114 was located near the $FMNH_2$ substrate, which allowed for stabilizing electrostatic interactions with the flavin, i.e., hydrogen bonding percent occupancy of up to 94% at an average distance of 2.7 Å (Table S2). Two new salt bridges were predicted with the mobile loop region in a closed conformation, that is, Asp111-Arg263 and Glu205-Arg271 with distances of 4.0 ± 0.2 Å for both interactions (Table 2 and Figure 3B). The Asp111-Arg263 and Glu205-Arg271 interactions had 67% and 60% hydrogen bonding percent occupancies, respectively, with distances of approximately 2.8 Å for the 1000 ns trajectories (Figure 4 and Table S1). In the open structure, the Arg263 and Arg271 residues were >19 Å away from Asp111 and Glu205

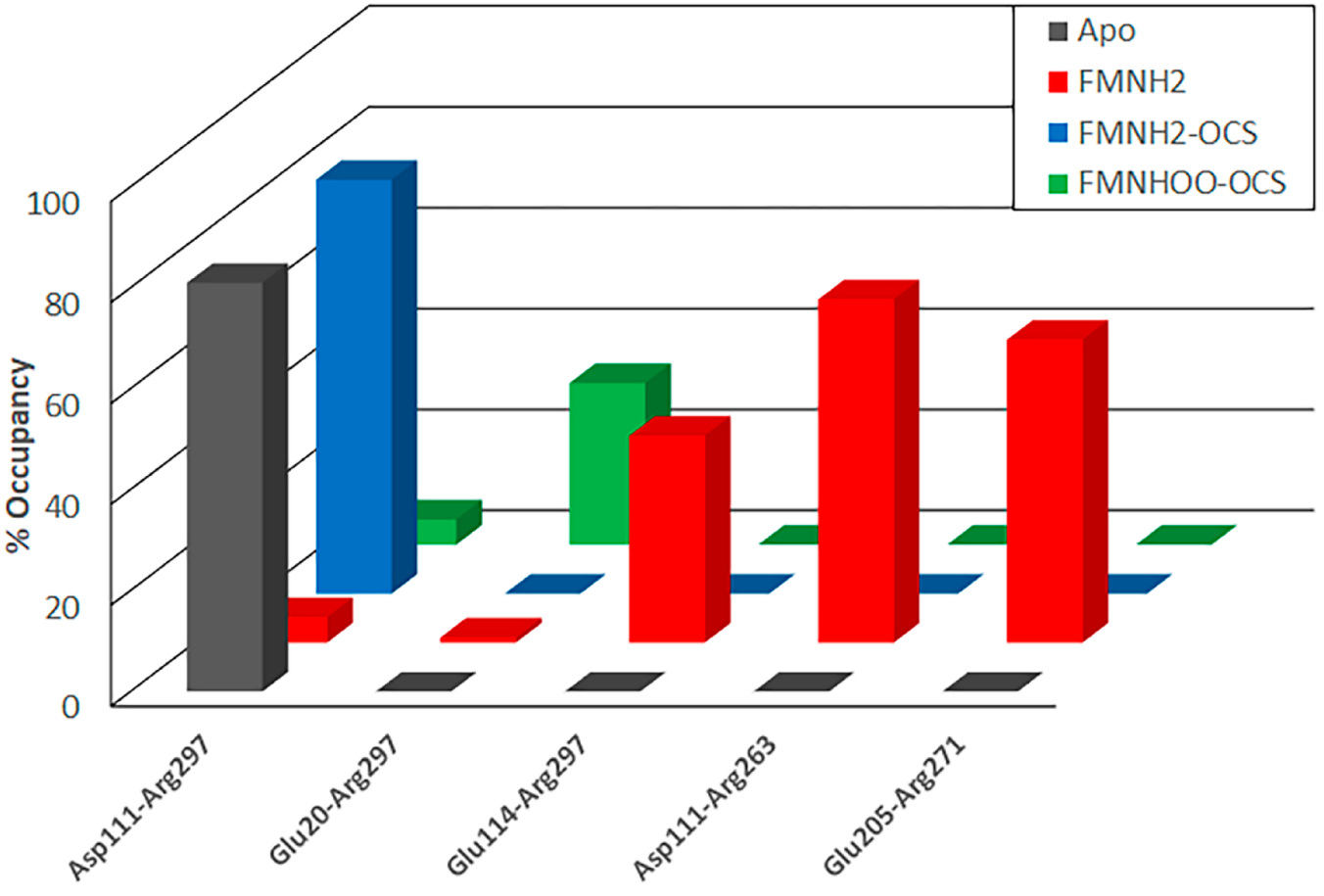

Figure 4. Hydrogen bonding percent occupancy between residues for the substrate-free and bound wild-type SsuD 1000 ns simulations.

https://dx.doi.org/10.1021/acs.biochem.0c00633
Biochemistry 2020, 59, 3582−3593

Table 3. Average Distances (in Å) between Residues for the SsuD Double Variant Systems Starting from a Closed Conformation Bound with $FMNH_2$

E205A/R271A	0−10 ns	290−300 ns	R263A/R271A	0−10 ns	590−600 ns
Asp111-Arg297	5.3 ± 0.5	5.5 ± 0.6	Asp111-Arg297	6 ± 1	7 ± 1
Glu20-Arg297	12 ± 1	14 ± 2	Glu20-Arg297	9 ± 3	10 ± 1
Glu114-Arg297	3.8 ± 0.1	4.0 ± 0.2	Glu114-Arg297	4.5 ± 0.5	4.1 ± 0.3
Asp111-Arg263	5 ± 2	3.9 ± 0.1	Asp111-Ala263	10 ± 2	9 ± 1
Ala205-Ala271	6 ± 1	15 ± 1	Glu205-Ala271	6 ± 1	16 ± 2

(Table 2). Interestingly, the Arg263 and Arg271 residues are conserved in methanesulfonate monooxygenase (MsuD). This could imply a special significance for the residues within the enzyme family, but further experimental investigation is required.

To further examine the potential role that Arg263 and Arg271 may play upon the closed mobile loop conformation, aMD simulations were performed for two additional $FMNH_2$-bound SsuD systems that possessed double substitutions. The first SsuD system had R263A and R271A substitutions and ran for 600 ns, whereas the second SsuD system had E205A and R271A substitutions and ran for 300 ns. The starting coordinates for systems with double substitutions were derived from the most dominant cluster in the 1000 ns trajectory of the closed $FMNH_2$-bound wild-type SsuD system (Figure S2). Simulations of the variants followed the same minimization and equilibration procedure as described in the methods section for the wild-type SsuD simulations. Table 3 provides the average distances between the key active site and mobile loop residues over the first and last 10 ns of the simulations for the $FMNH_2$-bound SsuD systems with double substitutions; distance plots over the entire trajectories are provided in Figure S5 and S6. As the R271A variant deleted the ability of SsuD to form a Glu205-Arg271 salt bridge (Figure 3B), both SsuD systems with double substitutions were deleteriously affected with a computed elongation in length between the residues from approximately 6 to 16 Å (Table 3). In the case of the Arg263 substitution, very interesting differences between the two double substitution systems were observed. In the E205A/R271A SsuD variant, the Asp111-Arg263 average distance tightened from 5 ± 2 Å at the beginning of the production run to 3.9 ± 0.1 Å during the final 10 ns. Whereas, for the R263A/R271A SsuD variant system, the new Asp111-Ala263 interaction immediately separated to a distance of 10 ± 2 Å within the first 10 ns of the production run and remained separated at 9 ± 1 Å at the end of the simulation (Table 3). Overall, the mobile loop region began to open up in response to the R263A/R271A double substitution with an angle of 36.6° between the active site plane and the mobile loop plane in the last frame of the 600 ns simulation (Figure S7) compared 7.3° for the $FMNH_2$-bound wild-type SsuD complex (Table 1).

Single and double substitutions of Arg263 and Arg271 to alanine (R263A, R271A, R263/271A SsuD) were generated to determine if the desulfonation activity of SsuD was affected by alterations in the salt bridge interactions. The single and double variants showed similar kinetic parameters as wild-type SsuD (Table 4). Previous studies have shown that wild-type SsuD is protected from proteolytic digestion in the presence of reduced FMN due to loop closure.[6] In the absence of reduced FMN, Arg297 is readily accessible to proteolytic digestion with trypsin. However, there was no change in the degree of protection with reduced FMN and octanesulfonate. Limited digestion of the R263A SsuD variant and reduced FMN with chymotrypsin showed comparable protection as wild-type (Figure 5). However, the R271A and R263A/R271A SsuD variants were not similarly protected. The lack of protection is likely due to the R271A SsuD substitution, as the level of protection was the same in the double variant. Therefore, although the kinetic parameters for the arginine variants were the same as wild-type, they were not equally protected. The decreased proteolytic protection seen with the R271A SsuD variants agrees with the computational findings. The increased distance between Glu205 and Ala271 results in a more open conformation leading to increased proteolysis.

Table 4. Steady-State Kinetic Parameter for the Variants and Wild-Type SsuD

	K_m, octanesulfonate (M, ×10^{-6})	k_{cat} (s^{-1})	k_{cat}/K_m (M^{-1} s^{-1}, ×10^{-4})
wild-type SsuD	50 ± 13	0.84 ± 0.06	1.7 ± 0.5
R263A SsuD	57 ± 8	1.40 ± 0.05	2.5 ± 0.4
R271A SsuD	235 ± 76	1.03 ± 0.14	0.44 ± 0.14
R263A/R271A SsuD	113 ± 31	1.10 ± 0.10	1.0 ± 0.3

Semiclosed Conformation. When wild-type SsuD was simultaneously bound with the $FMNH_2$ and OCS substrates, the system no longer adopted an open or closed conformation as defined earlier by obtuse or acute dihedral angles in the prior apo and $FMNH_2$-bound complexes, respectively. Instead, the calculation of the dihedral angle between the mobile loop and active site entrance planes yielded an approximate right angle of 89.5° for the most dominant cluster (Table 1), which is labeled here as a semiclosed conformation (Figure 6). In this orientation, the Asp111-Arg297 salt bridge interaction was computed to have a tight distance of 3.9 ± 0.2 Å (Table 2) with 82% hydrogen bonding occurring at an average distance of 2.8 Å between the residues over the 1000 ns simulation (Figure 4 and Table S1). The distance between Glu114-Arg297 of 6 ± 1 Å was found to be similar in length to the $FMNH_2$-bound SsuD system, i.e., 6 ± 2 Å. However, unlike the closed conformation, the Asp111-Arg263 and Glu205-Arg271 salt bridges in this semiclosed SsuD orientation did not form. Instead, distances of >14 Å were computed between the residue pairs (Table 2). The absence of the salt bridge pairs in the semiclosed conformation would explain the similar catalytic efficiency observed for each variant (Table 4). In the coupled assay, both reduced FMN and octanesulfonate are available, and the majority of the enzyme would be in the semiclosed state during turnover, so the Arg263 and Arg271 salt bridges would likely be a transient intermediate.

Spectrofluorimetric titration experiments have suggested that an $FMNH_2$-induced conformational change is essential to allow OCS to bind.[3] A subsequent second conformational change has been proposed upon the binding of OCS, which was supported by evidence from a rapid reaction kinetic

https://dx.doi.org/10.1021/acs.biochem.0c00633
Biochemistry 2020, 59, 3582−3593

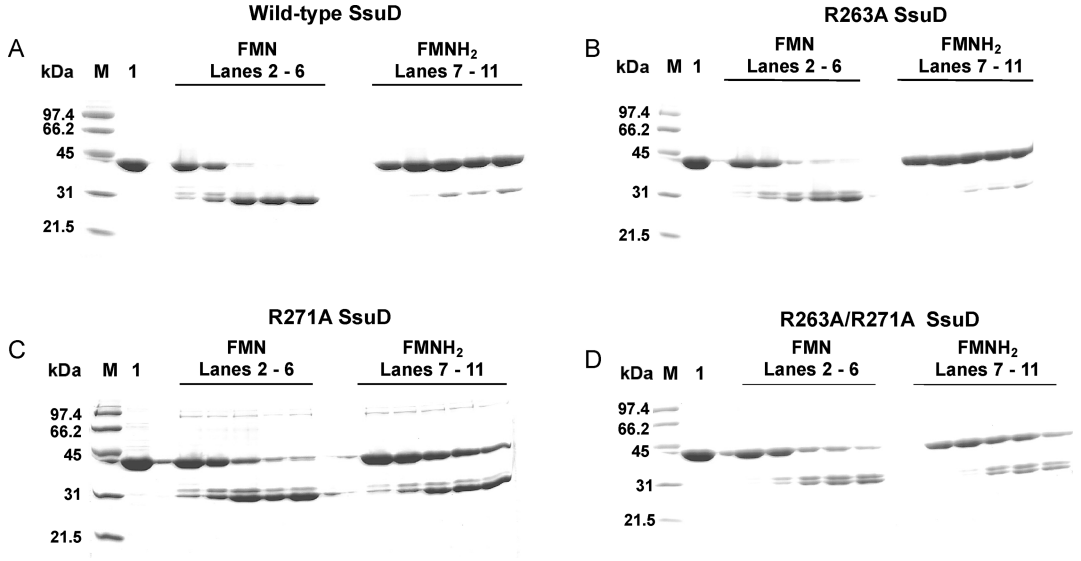

Figure 5. Proteolytic susceptibility of the variants and wild-type SsuD in the presence of FMN and $FMNH_2$. (A) Wild-type SsuD, (B) R263A SsuD, (C) R271A SsuD, (D) R263A/R271A SsuD. Gels A–D represent each enzyme incubated with FMN (lanes 2–6) and $FMNH_2$ (lanes 7–11). Gel lanes: molecular weight marker (M), SsuD standard (lane 1), aliquots were removed and quenched with PMSF after 0 s (lanes 2 and 7), 1 min (lanes 3 and 8), 5 min (lanes 4 and 9), 7 min (lanes 5 and 10), or 10 min (lanes 6 and 11)

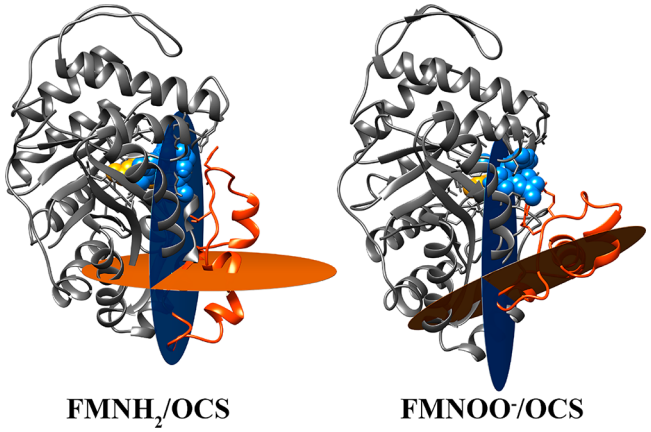

Figure 6. Top cluster structures for the $FMNH_2$/OCS-bound and $FMNOO^-$/OCS-bound SsuD complexes from the 1000 ns aMD simulation. The mobile loop plane is highlighted in orange and the active site entrance plane in blue.

analysis using alternate mixing of substrates.[7] It may be hypothesized from the current simulations that the first conformational change may be the closed conformation found when only $FMNH_2$ is bound to SsuD, perhaps used by the enzyme to avoid unproductive oxidation reactions. In previous studies, there was no change in the proteolytic susceptibility of wild-type SsuD with trypsin in the presence of $FMNH_2$ only and with both $FMNH_2$ and octanesulfonate.[6] Similar results were also observed with chymotrypsin (Figure S8A). However, the R271A SsuD variant with both reduced flavin and octanesulfonate was more protected with reduced flavin and octanesulfonate than with $FMNH_2$ alone (Figure S8B), lending further support that the absence of the salt bridge in the R271A SsuD variant with $FMNH_2$ leads to a more open conformation. When the Arg271 salt bridge no longer plays a role in the stabilization of conformations in the semiclosed state, the proteolytic susceptibility is similar to wild-type SsuD. The proteolytic experiments were performed under anaerobic conditions and may not represent the correct conformational state in the presence of dioxygen. In the presence of dioxygen, the closed conformation observed with $FMNH_2$ may not be formed as this conformational state would slow down catalysis. Upon the inclusion of octanesulfonate to the active site, i.e., $FMNH_2$/OCS, the second conformation (semiclosed) occurs that may be more appropriate for accepting dioxygen into the binding pocket or perhaps is better oriented for the ensuing oxygenolytic cleavage. For example, Arg226 has been reported to act as the active site acid in a proposed Baeyer–Villiger mechanism with variants of Arg226 possessing no detectable activity and no measurable formation of the $FMNOO^-$ intermediate.[51] Accordingly, in the semiclosed $FMNH_2$/OCS complex, the simulations found a hydrogen bond population density of 61% between OCS and Arg226 and 70% between Ser110 and $FMNH_2$ (Table S2). However, in the closed $FMNH_2$-bound SsuD system, Arg226 only H-bonded with $FMNH_2$ for 22% of the 1000 ns simulation.

A novel $\pi-\pi$ interaction involving His124 and Phe261 was found to occur with a computed distance of 5 ± 1 Å between the pair in the semiclosed conformation (Table 2). This interaction may aid in keeping water molecules from entering the catalytic pocket due to the presence of the bulky benzyl and imidazole moieties (Figure 7). To further examine the influence of His124 and Phe261 upon the semiclosed conformation, two additional 500 ns aMD simulations were carried out that featured either an F261A or F261W substitution in the $FMNH_2$/OCS bound SsuD complex. The starting coordinates for both variant systems were derived from the most dominant cluster in the 1000 ns trajectory of the semiclosed $FMNH_2$/OCS-bound wild-type SsuD system (Figure S2). The variant simulations followed the same minimization and equilibration procedure as described in the methods section for the wild-type SsuD simulations. Average distances between the key active site and mobile loop residues over the first and last 10 ns of the simulations for the F261A and F261W $FMNH_2$/OCS-bound SsuD systems are given in

https://dx.doi.org/10.1021/acs.biochem.0c00633
Biochemistry 2020, 59, 3582–3593

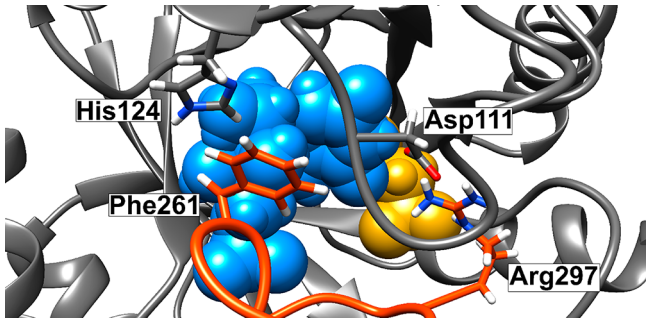

Figure 7. Illustration of the top cluster structure from the $FMNH_2$/OCS-bound SsuD 1000 ns aMD simulation. The mobile loop is colored in orange, and the $FMNH_2$ and OCS substrates are represented as space-filling models colored in blue and yellow, respectively.

Table 5; distance plots over the entire trajectories are provided in Figure S9 and S10.

The F261A SsuD simulation found that the His124-Ala261 interaction separated from 5 ± 1 Å to 30 ± 3 Å over the course of the 500 ns trajectory (Table 5). The mobile loop region completely opened with a computed obtuse dihedral angle of 110.9° between the active site and mobile loop planes for the most dominant cluster structure of F261A SsuD (Figure S11). The Asp111-Arg297 salt bridge was the only key residue−residue interaction that maintained a relatively close distance over the course of the simulations. Accordingly, an Asp111-Arg297 hydrogen bonding percent occupancy of 94% was found with an average H-bond distance of 2.80 Å (Table S3). These simulations highlight the importance of the His124-Phe261 in maintaining the semiclosed conformation. Consequently, it may be expected that an F261W SsuD variant would have little effect on the semiclosed conformation if the favorable $\pi-\pi$ interaction between His124 and the tryptophan residue is preserved. The F261W SsuD system had similar distances between key residues in the first and last 10 ns (Table 5). However, examining the distances between His124 and Trp261 for the SsuD variant over the entire 500 ns simulation found that the interaction did significantly separate between the 200 and 400 ns range with a value as large as 20.6 Å at 275 ns (Figure S10). In desulfonation assays performed here, the substitution of Phe261 with tryptophan inactivated SsuD with no sulfite detected.

The final simulation to be discussed is the SsuD system bound simultaneously with OCS and the C4a-peroxyflavin ($FMNOO^-$) intermediate proposed to form in the Baeyer−Villiger mechanism (Figure 8).[5] The top cluster structure had a computed dihedral angle of 66.8° between the active site entrance plane and the mobile loop plane (Table 1), which may suggest a semiclosed or closed conformation based on the acute angle; however, this conformation did not possess the residue interactions needed to shield the intermediate from solvent or to stabilize the substrates. For example, the simulations found very limited hydrogen bonding, 5%, between Asp111 and Arg297. In addition, the important His124-Phe261 interaction computed in the $FMNH_2$/OCS bound SsuD complex was not present for the $FMNOO^-$/OCS system, i.e., His124-Phe261 distance of 18 ± 6 Å (Table 2). Overall, the most dominant cluster structure in the $FMNOO^-$/OCS wild-type SsuD 1000 ns aMD simulation appeared to have an open mobile loop region (Figure 6) and, accordingly, the flavin intermediate exited the active site after approximately 900 ns. Triplicate simulation runs confirmed the results. It has been reported that the increased electrostatic environment of the active site prevents SsuD from adequately stabilizing the C4a-peroxyflavin intermediate, perhaps a consequence of the need for the enzyme to also stabilize the sulfonate functional group.[3] It may be speculated that $FMNOO^-$ is short-lived and would perhaps react with the octanesulfonate well before the semiclosed mobile loop conformation opened, expelling an oxidized form of flavin instead. Kinetic studies have reported that the oxygenated flavin intermediate is not observed at higher octanesulfonate concentrations.[3,7] Alternatively, it is possible that catalysis by SsuD could occur through a C4a-hydroperoxyflavin (FMNOOH) intermediate. Recently, an N5-peroxyflavin oxygenating intermediate has been proposed for the two-component flavin-dependent RutA enzyme.[52] It was suggested that some monooxygenase enzymes may employ an N5-peroxyflavin oxygenating intermediate for more challenging catalytic mechanisms. SsuD and other desulfonating enzymes (MsuD and SfnG) share similar structural features with RutA and may utilize a similar mechanism. Further mechanistic studies to evaluate the oxygenating flavin intermediate are warranted.

CONCLUSIONS

Loop structures in TIM-barrel proteins play a critical role in substrate binding and in the protection of reaction intermediates. Stabilization by the loop structure often occurs through specific interactions between conserved amino acids and substrate functional groups. Conformational changes observed in kinetic studies of SsuD have been attributed to the closure of the mobile loop region as a response to substrate binding.[3,7] Accelerated molecular dynamics simulations have been carried out to examine this possible correlation by studying SsuD at the atomic level bound with multiple combinations of $FMNH_2$, $FMNOO^-$, and OCS. Three distinct mobile loop conformations, open, closed, and semiclosed, were identified by the simulations and confirmed to be dependent upon the substrates bound in the active site, i.e., substrate-free, $FMNH_2$, and $FMNH_2$/OCS, respectively. To quantify the

Table 5. Average Distances (in Å) between Residues for the SsuD Variant Systems Starting from a Semiclosed Conformation Bound with $FMNH_2$ and OCS

F261A	0−10 ns	490−500 ns	F261W	0−10 ns	490−500 ns
His124-Ala261	5 ± 1	30 ± 3	His124-Trp261	4.2 ± 0.7	4.3 ± 0.4
Asp111-Arg297	4.0 ± 0.2	5.0 ± 0.7	Asp111-Arg297	5 ± 2	4.0 ± 0.2
Glu20-Arg297	20 ± 2	25 ± 1	Glu20-Arg297	18 ± 2	18 ± 1
Glu114-Arg297	7 ± 2	10 ± 1	Glu114-Arg297	7 ± 2	8 ± 1
Asp111-Arg263	16 ± 1	22.7 ± 0.6	Asp111-Ala263	17.4 ± 0.6	17 ± 0.5
Ala205-Ala271	14 ± 2	26 ± 2	Glu205-Ala271	14 ± 2	13 ± 2

https://dx.doi.org/10.1021/acs.biochem.0c00633
Biochemistry 2020, 59, 3582−3593

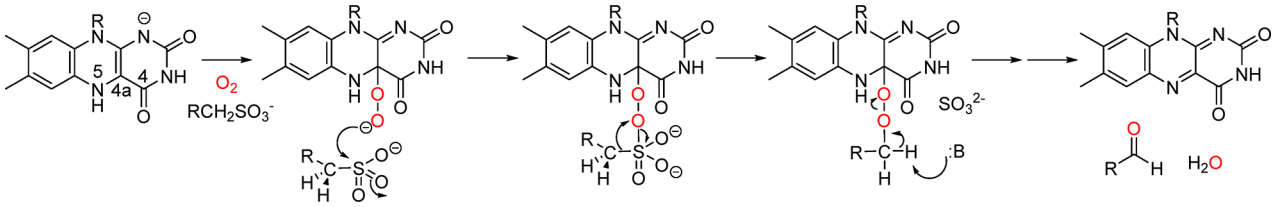

Figure 8. Proposed mechanism for desulfonation by SsuD involving a C4a-peroxyflavin. :B represents an active site amino acid that acts as a general base in catalysis.

differences between these conformations, a dihedral angle was computed by defining two planes to represent the active site entrance and the mobile loop of SsuD. A large obtuse dihedral angle of 122.8° between the planes was computed for the substrate-free wild-type SsuD system with a wide opening capable of providing full access for substrates to enter the active site. Upon binding $FMNH_2$ in SsuD, a conformational change occurred that possessed a substantial overlap between the planes with an acute angle of 7.8°. Multiple residues, including Arg297, Asp111, Arg271, Arg263, Glu205, and Glu114, were identified by the simulations to play a significant role in the conformations. SsuD Arg297 assists in loop closure by forming electrostatic interactions with the phosphate group of bound $FMNH_2$.[6,15] Enzymes with TIM-barrel structures that bind phosphate groups often contain a conserved basic residue on the loop that assists in closure.[24,53−55] In addition to Arg297, two salt bridges, Asp111-Arg263 and Glu205-Arg271, were found to be particularly important for maintaining the closed mobile loop conformation. Accordingly, simulations featuring an R263A and R271A double substitution predicted that the mobile loop region opened over time when starting from the closed conformation. Although single and double variants of Arg263 and Arg271 in SsuD were still experimentally active, the R271A and R263/271A SsuD variants were no longer protected from proteolytic digestion. Disruption of the salt bridge with the R271A SsuD variant led to a more "open" structure. It may be hypothesized from the current simulations that the "closed" conformation induced by $FMNH_2$ binding may be employed by the enzyme to avoid unproductive oxidation reactions in the absence of OCS.

When the wild-type SsuD enzyme was simultaneously bound with the $FMNH_2$ and OCS substrates, a second conformation was observed. This "semiclosed" orientation yielded an approximate right angle of 89.5° between the designated mobile loop and active site entrance planes. This conformation may be more appropriate for accepting O_2 into the binding pocket or perhaps may be better oriented for the ensuing oxygenolytic cleavage. A novel $\pi-\pi$ interaction between the His124 and Phe261 residues was predicted in this semiclosed orientation to prevent water molecules from entering the catalytic pocket due to the presence of the bulky benzyl and imidazole moieties. Simulations featuring either an F261A or F261W SsuD variant bound with the $FMNH_2$/OCS led the mobile loop region to completely open up with a computed obtuse dihedral angle of 110.9°. Accordingly, steady-state kinetic experiments performed on the F261W SsuD variant gave no observed activity. Finally, simulations on the wild-type SsuD system bound with OCS and the $FMNOO^-$ intermediate exhibited a computed dihedral angle of 66.8° between the planes but did not possess the residue interactions needed to shield the intermediate from solvent or to stabilize the substrates. It may be speculated that $FMNOO^-$ is short-lived and would perhaps react with the octanesulfonate well before the semiclosed mobile loop conformation opened. Given the potential for alternative flavin intermediates, e.g., N5-peroxyflavin or C4a-hydroperoxyflavin, further experimental mechanistic studies are warranted.

■ ASSOCIATED CONTENT

Supporting Information

The Supporting Information is available free of charge at https://pubs.acs.org/doi/10.1021/acs.biochem.0c00633.

RMSD versus time and between all pairs of frames; illustration of the top cluster structures and PDB files for wild-type and substituted SsuD; tables of hydrogen bonding percent occupancy; distances between residues for the SsuD variant simulations; illustration of the top cluster structure for R263A/R297A and F261A SsuD simulations; proteolytic susceptibility of R271A and wild-type SsuD; GAFF parameters for substrates (PDF)

PDB files (ZIP)

Accession Codes

Alkanesulfonate monooxygenase: P80645, *E. coli* SsuD. The SsuD variants were generated from P80645.

■ AUTHOR INFORMATION

Corresponding Author

Orlando Acevedo − *Department of Chemistry, University of Miami, Coral Gables, Florida 33146, United States;* orcid.org/0000-0002-6110-3930; Email: orlando.acevedo@miami.edu

Authors

Abhishek Thakur − *Department of Chemistry, University of Miami, Coral Gables, Florida 33146, United States*

Shruti Somai − *Department of Chemistry and Biochemistry, Auburn University, Auburn, Alabama 36849, United States*

Kun Yue − *Department of Chemistry, University of Miami, Coral Gables, Florida 33146, United States*

Nicole Ippolito − *Department of Chemistry, University of Miami, Coral Gables, Florida 33146, United States*

Dianne Pagan − *Department of Chemistry, University of Miami, Coral Gables, Florida 33146, United States*

Jingyuan Xiong − *West China School of Public Health and West China Fourth Hospital, Sichuan University, Chengdu 610041, China;* orcid.org/0000-0001-9354-862X

Holly R. Ellis − *Department of Chemistry and Biochemistry, Auburn University, Auburn, Alabama 36849, United States;* orcid.org/0000-0003-0521-422X

Complete contact information is available at: https://pubs.acs.org/10.1021/acs.biochem.0c00633

Notes

The authors declare no competing financial interest.

https://dx.doi.org/10.1021/acs.biochem.0c00633
Biochemistry 2020, 59, 3582−3593

■ ACKNOWLEDGMENTS

Gratitude is expressed to the National Science Foundation (CHE-1808495) and the University of Miami Center for Computational Sciences for support of this research.

■ ABBREVIATIONS

SsuD, alkanesulfonate monooxygenase; SsuE, alkanesulfonate flavin reductase; NAD(P)H, nicotinamide adenine dinucleotide (phosphate); FMN, flavin mononucleotide; $FMNH_2$, reduced flavin mononucleotide; $FMNOO^-$, C4a-peroxyflavin intermediate; OCS, octanesulfonate

■ REFERENCES

(1) Kertesz, M. A. (2000) Riding the sulfur cycle – metabolism of sulfonates and sulfate esters in Gram-negative bacteria. *FEMS Microbiol. Rev. 24*, 135–175.
(2) Kertesz, M. A., Leisinger, T., and Cook, A. M. (1993) Proteins induced by sulfate limitation in Escherichia coli, Pseudomonas putida, or Staphylococcus aureus. *J. Bacteriol. 175*, 1187–1190.
(3) Ellis, H. R. (2011) Mechanism for sulfur acquisition by the alkanesulfonate monooxygenase system. *Bioorg. Chem. 39*, 178–184.
(4) Eichhorn, E., van der Ploeg, J. R., and Leisinger, T. (1999) Characterization of a two-component alkanesulfonate monooxygenase from *Escherichia coli*. *J. Biol. Chem. 274*, 26639–26646.
(5) Armacost, K., Musila, J., Gathiaka, S., Ellis, H. R., and Acevedo, O. (2014) Exploring the Catalytic Mechanism of Alkanesulfonate Monooxygenase Using Molecular Dynamics. *Biochemistry 53*, 3308–3317.
(6) Carpenter, R. A., Xiong, J., Robbins, J. M., and Ellis, H. R. (2011) Functional role of a conserved arginine residue located on a mobile loop of alkanesulfonate monooxygenase. *Biochemistry 50*, 6469–6477.
(7) Zhan, X., Carpenter, R. A., and Ellis, H. R. (2008) Catalytic importance of the substrate binding order for the $FMNH_2$-dependent alkanesulfonate monooxygenase enzyme. *Biochemistry 47*, 2221–2230.
(8) Gao, B., and Ellis, H. R. (2007) Mechanism of flavin reduction in the alkanesulfonate monooxygenase system. *Biochim. Biophys. Acta, Proteins Proteomics 1774*, 359–367.
(9) Robbins, J. M., and Ellis, H. R. (2019) Investigations of two-component flavin-dependent monooxygenase systems. *Methods Enzymol. 620*, 399–422.
(10) Musila, J. M., Forbes, D. L., and Ellis, H. R. (2018) Functional Evaluation of the π-Helix in the NAD(P)H:FMN Reductase of the Alkanesulfonate Monooxygenase System. *Biochemistry 57*, 4469–4477.
(11) Driggers, C. M., Dayal, P. V., Ellis, H. R., and Karplus, P. A. (2014) Crystal Structure of Escherichia coli SsuE: Defining a General Catalytic Cycle for FMN Reductases of the Flavodoxin-like Superfamily. *Biochemistry 53*, 3509–3519.
(12) Abdurachim, K., and Ellis, H. R. (2006) Detection of protein-protein interactions in the alkanesulfonate monooxygenase system from *Escherichia coli*. *J. Bacteriol. 188*, 8153–8159.
(13) Dayal, P. V., Singh, H., Busenlehner, L. S., and Ellis, H. R. (2015) Exposing the Alkanesulfonate Monooxygenase Protein–Protein Interaction Sites. *Biochemistry 54*, 7531–7538.
(14) Jun, S. Y., Lewis, K. M., Youn, B., Xun, L., and Kang, C. (2016) Structural and biochemical characterization of EDTA monooxygenase and its physical interaction with a partner flavin reductase. *Mol. Microbiol. 100*, 989–1003.
(15) Eichhorn, E., Davey, C. A., Sargent, D. F., Leisinger, T., and Richmond, T. J. (2002) Crystal structure of *Escherichia coli* alkanesulfonate monooxygenase SsuD. *J. Mol. Biol. 324*, 457–468.
(16) Fisher, A. J., Raushel, F. M., Baldwin, T. O., and Rayment, I. (1995) Three-dimensional structure of bacterial luciferase from Vibrio harveyi at 2.4 Å resolution. *Biochemistry 34*, 6581–6586.
(17) Fisher, A. J., Thompson, T. B., Thoden, J. B., Baldwin, T. O., and Rayment, I. (1996) The 1.5-Å resolution crystal structure of bacterial luciferase in low salt conditions. *J. Biol. Chem. 271*, 21956–21968.
(18) Li, L., Liu, X., Yang, W., Xu, F., Wang, W., Feng, L., Bartlam, M., Wang, L., and Rao, Z. (2008) Crystal structure of long-chain alkane monooxygenase (LadA) in complex with coenzyme FMN: Unveiling the long-chain alkane hydroxylase. *J. Mol. Biol. 376*, 453–465.
(19) Sparks, J. M., and Baldwin, T. O. (2001) Functional Implications of the Unstructured Loop in the $(\beta/\alpha)8$ Barrel Structure of the Bacterial Luciferase α Subunit. *Biochemistry 40*, 15436–15443.
(20) Farber, G. K., and Petsko, G. A. (1990) The evolution of α/β barrel enzymes. *Trends Biochem. Sci. 15*, 228–234.
(21) Wierenga, R. K. (2001) The TIM-barrel fold: a versatile framework for efficient enzymes. *FEBS Lett. 492*, 193–198.
(22) AbouKhair, N. K., Ziegler, M. M., and Baldwin, T. O. (1985) Bacterial Luciferase: Demonstration of a Catalytically Competent Altered Conformational State following a Single Turnover. *Biochemistry 24*, 3942–3947.
(23) Xiong, J., and Ellis, H. R. (2012) Deletional studies to investigate the functional role of a dynamic loop region of alkanesulfonate monooxygenase. *Biochim. Biophys. Acta, Proteins Proteomics 1824*, 898–906.
(24) Malabanan, M. M., Amyes, T. L., and Richard, J. P. (2010) A role for flexible loops in enzyme catalysis. *Curr. Opin. Struct. Biol. 20*, 702–710.
(25) Carpenter, R. A., Zhan, X., and Ellis, H. R. (2010) Catalytic role of a conserved cysteine residue in the desulfonation reaction by the alkanesulfonate monooxygenase enzyme. *Biochim. Biophys. Acta, Proteins Proteomics 1804*, 97–105.
(26) Ferrario, V., Braiuca, P., Tessaro, P., Knapic, L., Gruber, C., Pleiss, J., Ebert, C., Eichhorn, E., and Gardossi, L. (2012) Elucidating the structural and conformational factors responsible for the activity and substrate specificity of alkanesulfonate monooxygenase. *J. Biomol. Struct. Dyn. 30*, 74–88.
(27) Liao, Q., Kulkarni, Y., Sengupta, U., Petrović, D., Mulholland, A. J., van der Kamp, M. W., Strodel, B., and Kamerlin, S. C. L. (2018) Loop Motion in Triosephosphate Isomerase Is Not a Simple Open and Shut Case. *J. Am. Chem. Soc. 140*, 15889–15903.
(28) Campbell, Z. T., Baldwin, T. O., and Miyashita, O. (2010) Analysis of the Bacterial Luciferase Mobile Loop by Replica-Exchange Molecular Dynamics. *Biophys. J. 99*, 4012–4019.
(29) Hamelberg, D., Mongan, J., and McCammon, J. A. (2004) Accelerated molecular dynamics: A promising and efficient simulation method for biomolecules. *J. Chem. Phys. 120*, 11919–11929.
(30) Pierce, L. C. T., Salomon-Ferrer, R., de Oliveira, C. A. F., McCammon, J. A., and Walker, R. C. (2012) Routine Access to Millisecond Time Scale Events with Accelerated Molecular Dynamics. *J. Chem. Theory Comput. 8*, 2997–3002.
(31) Eswar, N., Marti-Renom, A., Webb, B., Madhusudhan, M. S., Eramian, D., Shen, M., Pieper, U., and Sali, A. (2006) Comparative Protein Structure Modeling with MODELLER, In *Current Protocols in Bioinformatics*, pp 5.6.1–5.6.30, John Wiley & Sons, Inc.
(32) Trott, O., and Olson, A. J. (2009) AutoDock Vina: Improving the Speed and Accuracy of Docking with a New Scoring Function, Efficient Optimization and Multithreading. *J. Comput. Chem. 31*, 455–461.
(33) Hamelberg, D., Oliveira, C. A. F. D., and McCammon, J. A. (2007) Sampling of slow diffusive conformational transitions with accelerated molecular dynamics. *J. Chem. Phys. 127*, 155102.
(34) Bucher, D., Pierce, L. C. T., McCammon, J. A., and Markwick, P. R. L. (2011) On the Use of Accelerated Molecular Dynamics to Enhance Configurational Sampling in Ab Initio Simulations. *J. Chem. Theory Comput. 7*, 890–897.
(35) Miao, Y., Sinko, W., Pierce, L., Bucher, D., Walker, R. C., and McCammon, J. A. (2014) Improved Reweighting of Accelerated Molecular Dynamics Simulations for Free Energy Calculation. *J. Chem. Theory Comput. 10*, 2677–2689.

https://dx.doi.org/10.1021/acs.biochem.0c00633
Biochemistry 2020, 59, 3582–3593

(36) Gedeon, P. C., Thomas, J. R., and Madura, J. D. (2015) Accelerated Molecular Dynamics and Protein Conformational Change: A Theoretical and Practical Guide Using a Membrane Embedded Model Neurotransmitter Transporter, In *Molecular Modeling of Proteins. Methods in Molecular Biology* (Kukol, A., Ed.), pp 253−287, Humana Press, New York, NY.
(37) Salomon-Ferrer, R., Case, D. A., and Walker, R. C. (2013) An overview of the Amber biomolecular simulation package. *WIREs Comput. Mol. Sci. 3*, 198−210.
(38) Jorgensen, W. L., Chandrasekhar, J., Madura, J. D., Impey, W., and Klein, M. L. (1983) Comparison of simple potential functions for simulating liquid water. *J. Chem. Phys. 79*, 926−935.
(39) Hornak, V., Abel, R., Okur, A., Strockbine, B., Roitberg, A., and Simmerling, C. (2006) Comparison of Multiple Amber Force Fields and Development of Improved Protein Backbone Parameters. *Proteins: Struct., Funct., Genet. 65*, 712−725.
(40) Maier, J. A., Martinez, C., Kasavajhala, K., Wickstrom, L., Hauser, K. E., and Simmerling, C. (2015) ff14SB: Improving the Accuracy of Protein Side Chain and Backbone Parameters from ff99SB. *J. Chem. Theory Comput. 11*, 3696−3713.
(41) Wang, J., Wolf, R. M., Caldwell, J. W., Kollman, P. A., and Case, D. A. (2004) Development and Testing of a General Amber Force Field. *J. Comput. Chem. 25*, 1157−1174.
(42) Jorgensen, W. L. (1998) BOSS - Biochemical and Organic Simulation System, In *Encyclopedia of Computational Chemistry* (Schleyer, R., Ed.), pp 3281−3285, John Wiley & Sons Ltd., Athens, USA.
(43) Jorgensen, W. L., Maxwell, D. S., and Tirado-Rives, J. (1996) Development and testing of the OPLS all-atom force field on conformational energetics and properties of organic liquids. *J. Am. Chem. Soc. 118*, 11225−11236.
(44) Frisch, M. J. (2009) *Gaussian 09*, Revision B.01, Wallingford, CT.
(45) Le Grand, S., Goetz, A. W., and Walker, R. C. (2013) SPFP: Speed without compromise - a mixed precision model for GPU accelerated molecular dynamics simulations. *Comput. Phys. Commun. 184*, 374−380.
(46) Salomon-Ferrer, R., Goetz, A. W., Poole, D., Le Grand, S., and Walker, R. C. (2013) Routine microsecond molecular dynamics simulations with AMBER - Part II: Particle Mesh Ewald. *J. Chem. Theory Comput. 9*, 3878−3888.
(47) Michaud-Agrawal, N., Denning, E. J., Woolf, T. B., and Beckstein, O. (2011) MDAnalysis: A toolkit for the analysis of molecular dynamics simulations. *J. Comput. Chem. 32*, 2319−2327.
(48) Roe, D. R., and Cheatham, T. E., III (2013) PTRAJ and CPPTRAJ: Software for Processing and Analysis of Molecular Dynamics Trajectory Data. *J. Chem. Theory Comput. 9*, 3084−3095.
(49) Shao, J., Tanner, S. W., Thompson, N., and Cheatham, T. E., III (2007) Clustering Molecular Dynamics Trajectories: 1. Characterizing the Performance of Different Clustering Algorithms. *J. Chem. Theory Comput. 3*, 2312−2334.
(50) Grossfield, A., Patrone, P. N., Roe, D. R., Schultz, A. J., Siderius, D. W., and Zuckerman, D. M. (2019) Best Practices for Quantification of Uncertainty and Sampling Quality in Molecular Simulations. *Living J. Comp. Mol. Sci. 1*, 5067.
(51) Robbins, J. M., and Ellis, H. R. (2012) Identification of critical steps governing the two-component alkanesulfonate monooxygenase catalytic mechanism. *Biochemistry 51*, 6378−6387.
(52) Matthews, A., Saleem-Batcha, R., Sanders, J. N., Stull, F., Houk, K. N., and Teufel, R. (2020) Aminoperoxide adducts expand the catalytic repertoire of flavin monooxygenases. *Nat. Chem. Biol. 16*, 556−563.
(53) Lolis, E., and Petsko, G. A. (1990) Crystallographic analysis of the complex between triosephosphate isomerase and 2-phosphoglycolate at 2.5-Å resolution: implications for catalysis. *Biochemistry 29*, 6619−6625.
(54) Davenport, R. C., Bash, P. A., Seaton, B. A., Karplus, M., Petsko, G. A., and Ringe, D. (1991) Structure of the triosephosphate isomerase-phosphoglycolohydroxamate complex: an analogue of the intermediate on the reaction pathway. *Biochemistry 30*, 5821−5826.
(55) Miller, B. G., Snider, M. J., Short, S. A., and Wolfenden, R. (2000) Contribution of enzyme-phosphoribosyl contacts to catalysis by orotidine 5′-phosphate decarboxylase. *Biochemistry 39*, 8113−8118.

https://dx.doi.org/10.1021/acs.biochem.0c00633
Biochemistry 2020, 59, 3582−3593